AMERICAN SOCIETY FOR MICROBIOLOGY | mBio®

RESEARCH ARTICLE

The Pearling Transition Provides Evidence of Force-Driven Endosomal Tubulation during *Salmonella* Infection

Yunfeng Gao,[a] Christoph Spahn,[b] Mike Heilemann,[b] Linda J. Kenney[a,c,d,e]

[a]Mechanobiology Institute, National University of Singapore, Singapore, Singapore
[b]Institute of Physical and Theoretical Chemistry, Johann Wolfgang Goethe-University, Frankfurt, Germany
[c]Department of Biochemistry, National University of Singapore, Singapore, Singapore
[d]Jesse Brown VA Medical Center, Chicago, Illinois, USA
[e]Department of Microbiology and Immunology, University of Illinois—Chicago, Chicago, Illinois, USA

ABSTRACT Bacterial pathogens exploit eukaryotic pathways for their own end. Upon ingestion, *Salmonella enterica* serovar Typhimurium passes through the stomach and then catalyzes its uptake across the intestinal epithelium. It survives and replicates in an acidic vacuole through the action of virulence factors secreted by a type three secretion system located on *Salmonella* pathogenicity island 2 (SPI-2). Two secreted effectors, SifA and SseJ, are sufficient for endosomal tubule formation, which modifies the vacuole and enables *Salmonella* to replicate within it. Two-color, superresolution imaging of the secreted virulence factor SseJ and tubulin revealed that SseJ formed clusters of conserved size at regular, periodic intervals in the host cytoplasm. Analysis of SseJ clustering indicated the presence of a pearling effect, which is a force-driven, osmotically sensitive process. The pearling transition is an instability driven by membranes under tension; it is induced by hypotonic or hypertonic buffer exchange and leads to the formation of beadlike structures of similar size and regular spacing. Reducing the osmolality of the fixation conditions using glutaraldehyde enabled visualization of continuous and intact tubules. Correlation analysis revealed that SseJ was colocalized with the motor protein kinesin. Tubulation of the endoplasmic reticulum is driven by microtubule motors, and in the present work, we describe how *Salmonella* has coopted the microtubule motor kinesin to drive the force-dependent process of endosomal tubulation. Thus, endosomal tubule formation is a force-driven process catalyzed by *Salmonella* virulence factors secreted into the host cytoplasm during infection.

IMPORTANCE This study represents the first example of using two-color, superresolution imaging to analyze the secretion of *Salmonella* virulence factors as they are secreted from the SPI-2 type three secretion system. Previous studies imaged effectors that were overexpressed in the host cytoplasm. The present work reveals an unusual force-driven process, the pearling transition, which indicates that *Salmonella*-induced filaments are under force through the interactions of effector molecules with the motor protein kinesin. This work provides a caution by highlighting how fixation conditions can influence the images observed.

KEYWORDS kinesin, *Salmonella* Typhimurium, *Salmonella*-induced filaments, SseJ, endosomal tubulation, pearling transition, superresolution microscopy

After ingestion from contaminated food or water, *Salmonella enterica* serovar Typhimurium passes through the stomach and is taken up across the intestinal epithelium. Subsequently, *Salmonella* resides in an acidic vacuole, which it modifies to prevent phagosome-lysosome fusion and elimination (1). A specialized type three secretory system, encoded on *Salmonella* pathogenicity island 2 (SPI-2), is induced by

Received 17 May 2018 **Accepted** 21 May 2018 **Published** 19 June 2018

Citation Gao Y, Spahn C, Heilemann M, Kenney LJ. 2018. The pearling transition provides evidence of force-driven endosomal tubulation during *Salmonella* infection. mBio 9:e01083-18. https://doi.org/10.1128/mBio.01083-18.

Editor Tarek Msadek, Institut Pasteur

Address correspondence to Mike Heilemann, heilemann@chemie.uni-frankfurt.de, or Linda J. Kenney, kenneyl@uic.edu.

Y.G. and C.S. contributed equally to this work.

This article is a direct contribution from a Fellow of the American Academy of Microbiology. Solicited external reviewers: Markus Sauer, University of Wurzburg; Stanley Maloy, San Diego State University.

the acid pH of the vacuole, driving secretion of bacterial factors that modify host functions (2). Thus, through its secreted virulence factors (referred to as effectors), *Salmonella* can survive and replicate inside cells and eventually is disseminated to the liver and spleen. Intracellular survival of *Salmonella* is promoted through the concerted action of SifA (*Salmonella*-induced filaments [SIFs]) and its counter effector SseJ (3–5). Formation of SIFs is not well understood, due in part to the limitations of imaging. In the present work, we used superresolution imaging to visualize the secreted effector SseJ during infection and discovered that *in vivo* forces transmitted by the motor protein kinesin are involved in endosomal trafficking induced by *Salmonella*.

Superresolution microscopy allows visualization of biological structures at scales far below the diffraction limit of light (6). We applied single-molecule localization microscopy (SMLM) (7) to visualize the virulence factor SseJ in the host cytosol after *Salmonella* infection. A limitation of previous studies is that they examined effectors overexpressed in the cytoplasm of tissue culture cells (5, 8–10). In the present work, we visualize SseJ using superresolution imaging upon its secretion from the bacterial SPI-2 type three secretion system. We examined the distribution of SseJ with respect to the late endosomal marker LAMP-1, tubulin, or kinesin, using two-color superresolution imaging. Our results indicate that SseJ clustering appears to be an event driven by the pearling transition, and clusters are exquisitely sensitive to fixation.

The pearling transition or instability is a sequential beading of tubular vesicles, first observed in preparations of endoplasmic reticulum (ER) membranes that were shown to be sensitive to hypotonic solutions (11). Pearling can also be driven by high osmolality (12, 13). Axons were reshaped during osmotic shock (14), and theoretical biophysical models describing membrane tubulation were developed (15). Previous microscopy studies of *Salmonella* secreted effectors used 4% paraformaldehyde (PFA) at high osmolality (748 mosmol/kg) for fixation (16). In the present work, we show that under low-osmolality fixation conditions (0.2% glutaraldehyde [GA], 282 mosmol/kg), which preserve the structure of microtubules, pearls of SseJ are no longer evident. Instead, SseJ is visible as a continuous filament. Thus, the view of endosomal tubulation needs revision, based on fixation conditions that preserve tubular structures. The pearling transition also reveals a force-dependent process that drives endosomal tubulation, and here we identify kinesin as the motor that supplies this force (17).

RESULTS

Visualizing a secreted virulence factor by superresolution imaging. In the past, effector proteins have been visualized after overexpression in the host cytoplasm in the absence of the pathogen and in isolation from other virulence factors (5, 8–10). Confocal microscopy was generally employed for this analysis. We constructed a *Salmonella* strain expressing an SseJ-hemagglutinin (HA) tag and demonstrated that this strain was competent for SPI-2-dependent SseJ secretion (2). We then used this strain to infect HeLa cells (see Materials and Methods). At 10 and 12 h postinfection, we fixed the cells with paraformaldehyde (PFA) and performed superresolution imaging (Fig. 1). SseJ-HA (red) was readily apparent as a mixture of regular, periodic clusters (Fig. 1a, ii and iii) and as filamentous structures (Fig. 1b, ii and iii). *Salmonella*-induced filaments form because *Salmonella*-secreted effectors coopt LAMP-1-positive endosomes to form long, fused tubules. It is hypothesized that endosomal tubulation provides membrane and nutrients for the expanding vacuole, allowing *Salmonella* to replicate inside the vacuole during infection.

SseJ forms clusters in the host cytoplasm. SseJ-HA formed uniform clusters that were apparent as ringlike structures that colocalized with LAMP-1 (Fig. 1). Analysis of the SseJ clusters revealed that they were periodic, with an average spacing between ~1 and 2 μm, and of a uniform size ranging from 200 to 400 nm (Fig. 2). A closeup of LAMP-1 endosomes clearly indicated that SseJ and LAMP-1 were colocalized (Fig. 1 and 2). The regular spacing of SseJ clusters led us to probe the molecular mechanism leading to cluster periodicity.

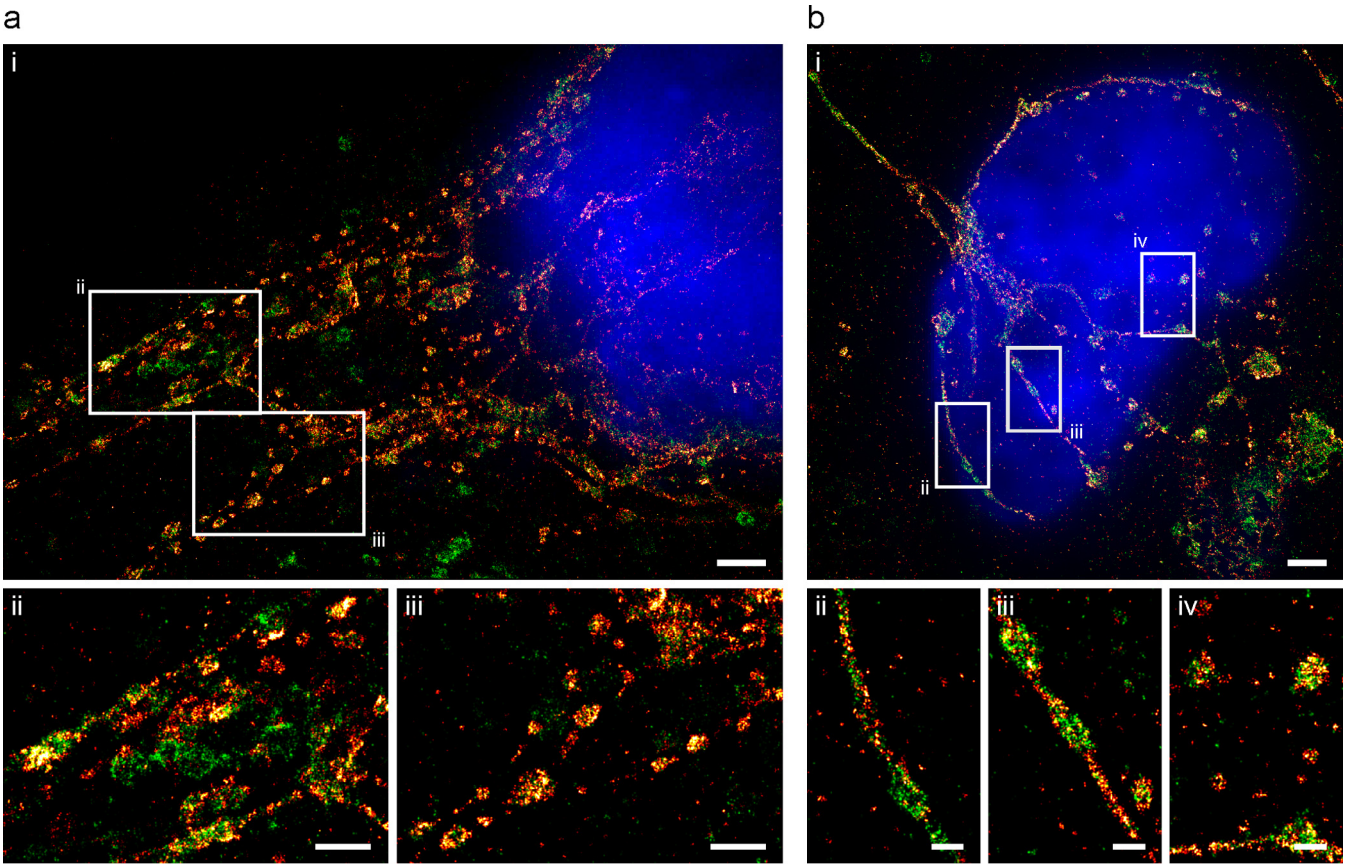

FIG 1 Distribution of *Salmonella* effector protein SseJ-HA and LAMP-1 in PFA-fixed HeLa cells. (a) Dual-color *d*STORM image of an infected cell, 10 h after invasion. Both filamentous (ii) and vesicular (iii) structures of SseJ-HA (red) that colocalize with the host cell protein LAMP-1 (green) are observed. Host nuclei are stained with 4′,6-diamidino-2-phenylindole (DAPI; blue). (b) Dual-color *d*STORM image of an infected HeLa cell, 12 h after invasion, highlighting the appearance of filamentous structures (ii and iii) as well as clusters of SseJ (iv). Bars, 2 μm (ai and bi) and 1 μm (aii, aiii, and bii to iv).

SseJ colocalizes with tubulin. We imaged SseJ together with β-tubulin, which forms continuous filaments with a defined width of ~25 nm (Fig. 3). SseJ clusters were evident at regular intervals along the microtubules and were similar in size and spacing to the LAMP-1-colocalized clusters shown in Fig. 2. However, it was apparent that the microtubules were disrupted and were not well preserved. Structural preservation of microtubules depends on the fixative, and they are better preserved in glutaraldehyde (GA) than in paraformaldehyde (PFA) (18). We thus questioned whether SseJ clusters were a result of fixation conditions that disrupted the endosomal tubules.

SIFs are also subject to fixation conditions. We repeated *Salmonella* infections and employed GA fixation conditions to image SseJ (18). Interestingly, GA fixation altered the pattern of SseJ, in which continuous filaments were now evident, with a uniform distribution of SseJ along the filaments (Fig. 4a; see also Fig. S1 and S2 in the supplemental material). These filamentous tubules had a diameter of 157 $\pm$ 3 nm (Fig. 4b, c, and d), similar to tubular structures visualized by electron microscopy (EM) (19). This result suggested that the clusters of SseJ observed in the PFA-fixed cells (Fig. 1 to 3) were not representative of native structures and that the native structures were disrupted by fixation. It is worth emphasizing here that in the present study, we analyzed *Salmonella*-expressed effector proteins directly after secretion, rather than overexpressing effector proteins in the host cytoplasm.

The pearling transition drives SseJ clustering. Membranes under tension can undergo an instability known as the pearling transition, induced by hypotonic buffer exchange and leading to the formation of beadlike structures of similar size and regular spacing (11). While the first report described the pearling effect during hypotonic buffer

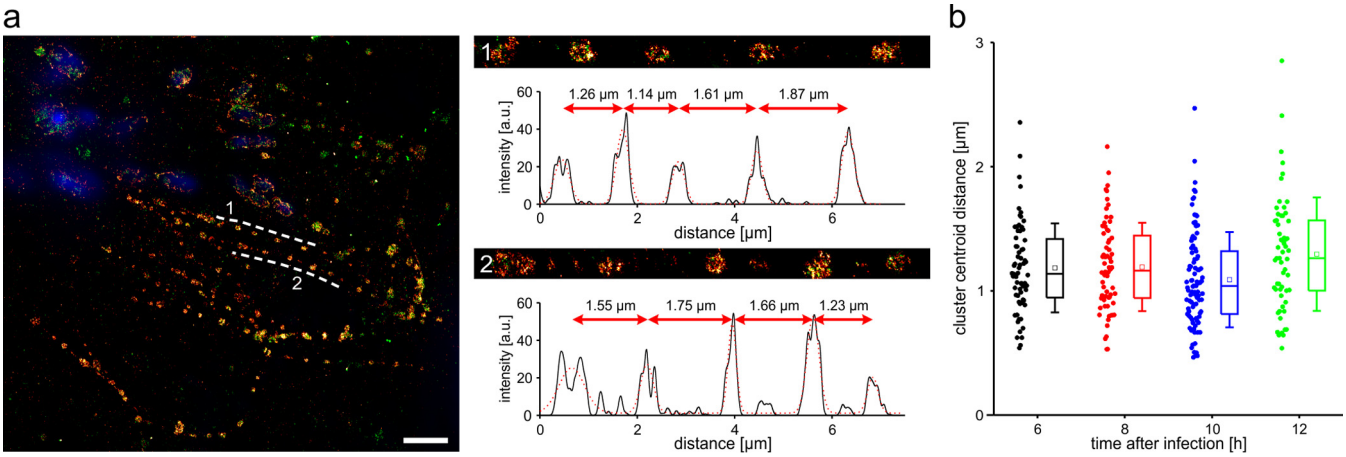

FIG 2 Clusters of SseJ appear regular in size and are periodically spaced. (a) Representative *d*STORM image of a HeLa cell infected with *Salmonella* 10 h postinfection. After infection, HeLa cells were fixed with PFA and labeled with SseJ-HA (red) and LAMP-1 (green), and DNA (*Salmonella* nucleoids) was labeled with DAPI (blue). SseJ clusters appear as pearls on a string (indicated by dashed lines) with a typical spacing of 1 to 2 μm. The straightened course and respective intensity profiles and the distances between clusters along the dashed lines are shown on the right (panels 1 and 2). a.u., arbitrary units. (b) The cluster spacing did not change over time during *Salmonella* infection. The data points represent single cluster distances, while the boxes show the percentiles, the horizontal lines represent the medians, the empty squares are the mean values, and the whiskers are the standard deviations. For each time point, 4 to 5 cells from two independent infections were analyzed, resulting in 59 to 94 individual spacings from 11 to 20 pearls-on-a-string structures. The mean clusters of the centroid distances were determined to be 1.18 $\pm$ 0.04 μm (standard error of the mean) (6 h, $n = 68$), 1.19 $\pm$ 0.04 μm (8 h, $n = 68$), 1.09 $\pm$ 0.04 μm (10 h, $n = 94$), and 1.29 $\pm$ 0.06 μm (12 h, $n = 59$). Bar, 3 μm.

exchange (11), we observed the formation of regularly spaced SseJ clusters after an osmotic upshift (Fig. 1 to 3, S1, and S2). Similar effects were also reported for lipid vesicles (12, 13, 20). In HeLa cells infected with *Salmonella* and fixed with PFA, we observed periodic spacing and a uniform cluster size of SseJ (Fig. 1–3). Surprisingly, these clusters were absent in cells fixed with GA (Fig. 4). We interpret this altered appearance as a pearling effect induced by the differing osmolality of the fixation buffers (748 mosmol/kg in PFA compared to 282 mosmol/kg in GA). However, in order for a pearling effect to occur, a force is required that exerts a tension on the *Salmonella* filaments experienced by SseJ.

Kinesin supplies the motor force that drives pearling as well as endosomal tubulation. *Salmonella*-secreted effector SifA was reported to interact with kinesin-1 through an adapter protein, SKIP (17). Because of the close proximity of SseJ and tubulin (Fig. 3 and S2), we speculated that kinesin might also be closely associated with SseJ. We performed spinning-disk structured illumination microscopy (SIM) (21) and examined the pattern of kinesin and SseJ (Fig. 5). Kinesin was present at high density throughout the cytoplasm, and SseJ appeared in close proximity to kinesin. In order to determine whether these two proteins were colocalized, we modified Manders colocalization analysis (22) for dense protein patterns (see Materials and Methods for a detailed description) and obtained strong evidence of positive colocalization (Fig. 5b). In contrast, a mock infection provided the background for the absence of an SseJ-kinesin interaction (Fig. 5b). Further evidence supporting a kinesin-SseJ interaction was provided by similar analysis in a mutant strain lacking *sifA*, the partner effector of SseJ. In this background, SseJ surrounded the vacuole, since the absence of *Salmonella*-induced filaments did not enable SseJ trafficking (Fig. S3). Because SseJ and kinesin were colocalized (Fig. 5), and SseJ was sensitive to osmolality-induced pearling, we propose that kinesin exerts an indirect force on SseJ located on endosomal tubules. This is likely a weak interaction, i.e., one that is easily disrupted by fixation, since SseJ colocalization with kinesin has not been previously observed.

DISCUSSION

Pearling appears as a finite-amplitude, peristaltic modulation of a cylinder, characterized by a well-defined wavelength. Isolated spherical pearls of clustered LAMP-1-

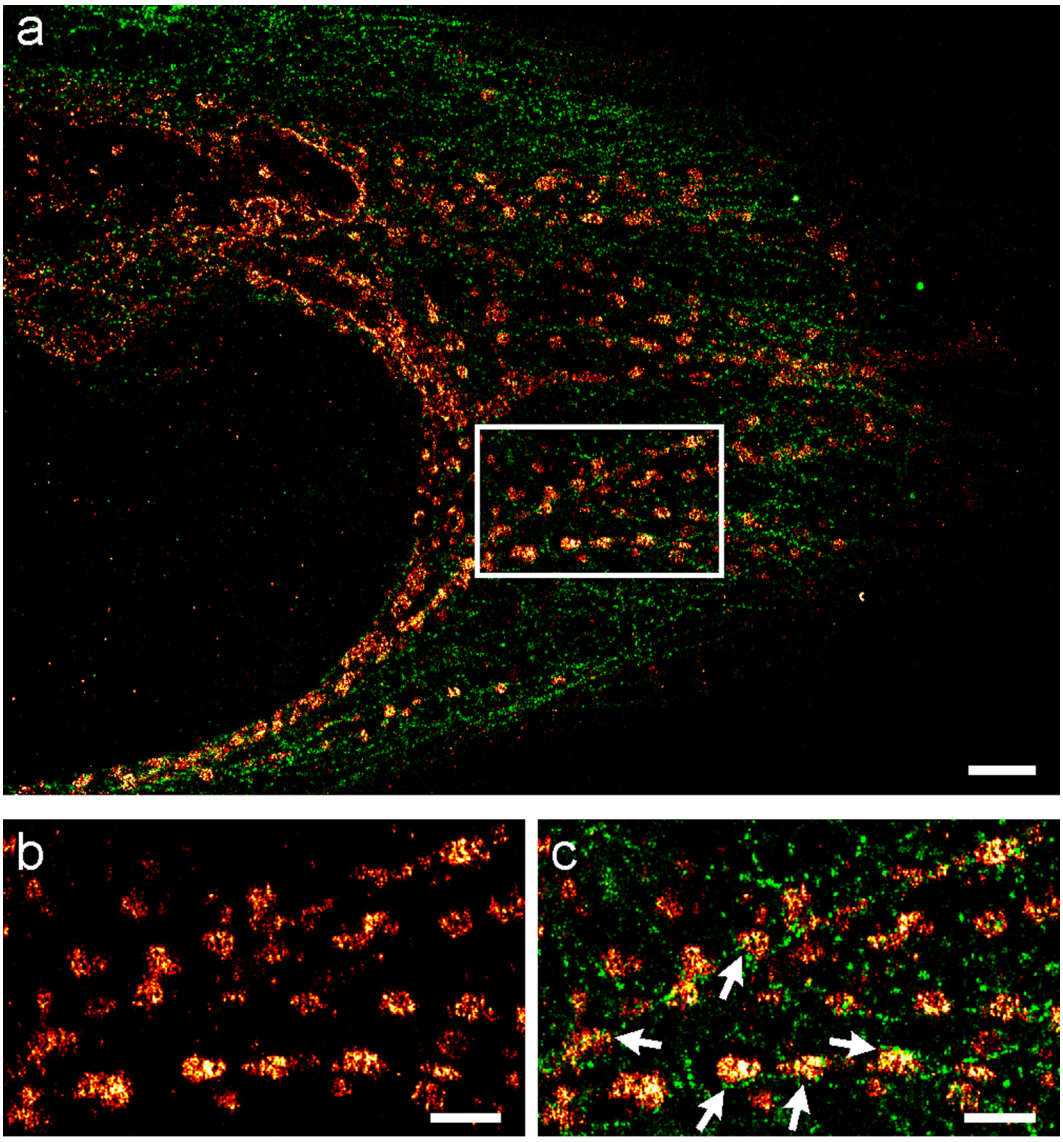

FIG 3 SseJ colocalizes with tubulin. (a) Dual-color *d*STORM image of an infected HeLa cell (8 h postinfection), fixed with PFA and stained for SseJ (red) and tubulin (green). (b and c) Magnified view of the boxed region in panel a shows that SseJ is mainly found in small clusters adjacent to tubulin filaments (white arrows indicate close proximity [c]). Bars, 2 μm (a) and 1 μm (b and c).

positive SIFs drive clustering of SseJ molecules. Pearling occurs predominantly in thinner tubes (23), which may explain why pearls were not observed at later times during infection. As the SIFs elongate, thicken, and morph into a double-membrane tubule, SseJ distribution also becomes filamentous (compare Fig. 1a and 2 with 1b). Membrane tension, which initiates the instability, is often induced by elongation (23), which in this case is driven through contacts via SseJ and kinesin to microtubules. Although a direct interaction of SifA and SseJ has not been demonstrated (5), both SseJ and SifA are known to interact with RhoA (24). Thus, RhoA may be the adapter that links SseJ with SifA and SKIP to kinesin. In the *sifA* deletion strain, SIFs are absent and SseJ remains associated with the vacuole (see Fig. S3 in the supplemental material).

A diagram of the events involved in SseJ clustering is provided in Fig. 6. When *Salmonella* resides in the vacuole, the sensor kinase EnvZ senses the acidic environment and drives OmpR-dependent acidification to pH 5.6 (2, 25). This leads to the upregulation of the SsrA/B two-component system located on SPI-2, and SsrB binding to DNA increases by 50%, driving the expression of SPI-2 type three secretion structural genes

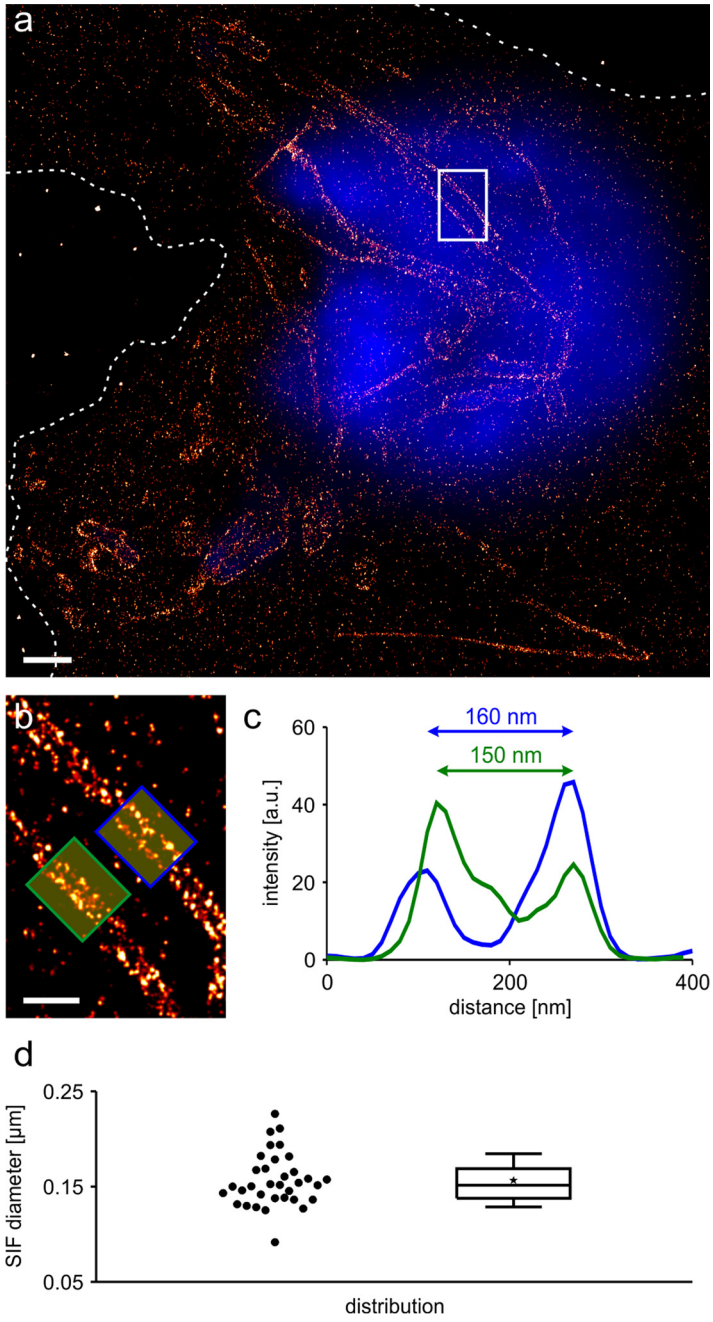

FIG 4 SseJ appears as continuous filaments in GA-fixed cells. (a) Representative image of a HeLa cell infected with *Salmonella* (12 h after invasion), fixed with GA, and stained for SseJ-HA (red) and host and *Salmonella* DNA (blue). Dashed lines indicate the cell boundaries. (b) A magnified view of the boxed region in panel a shows SIFs. (c) The cross-sectional intensity profile of the two filaments shown in panel b reveals SIF diameters of 150 to 160 nm. (d) Distribution of measured SIF diameters. Data points represent single diameters, while the boxes show the percentiles, the horizontal line shows the median, the asterisk shows the mean value, and whiskers show the standard deviations. Six cells from three independent infections were analyzed, resulting in 34 cross-sectional diameters from 23 individual SIFs. The mean diameter was determined to be 157 ± 3 nm. Bars, 2 μm (a) and 0.5 μm (b).

and effectors (A. Liew et al., submitted for publication) (Fig. 6, top). Kinesin interacts with a complex of SKIP, SifA, and SseJ, pulling the vacuolar membrane along microtubules and incorporating LAMP-1 endosomes into the SIFs. Under PFA fixation conditions, SseJ is observed as regularly spaced clusters at fixed intervals. At lower osmolality, pearling does not occur and SseJ is continuously observed all along the SIFs.

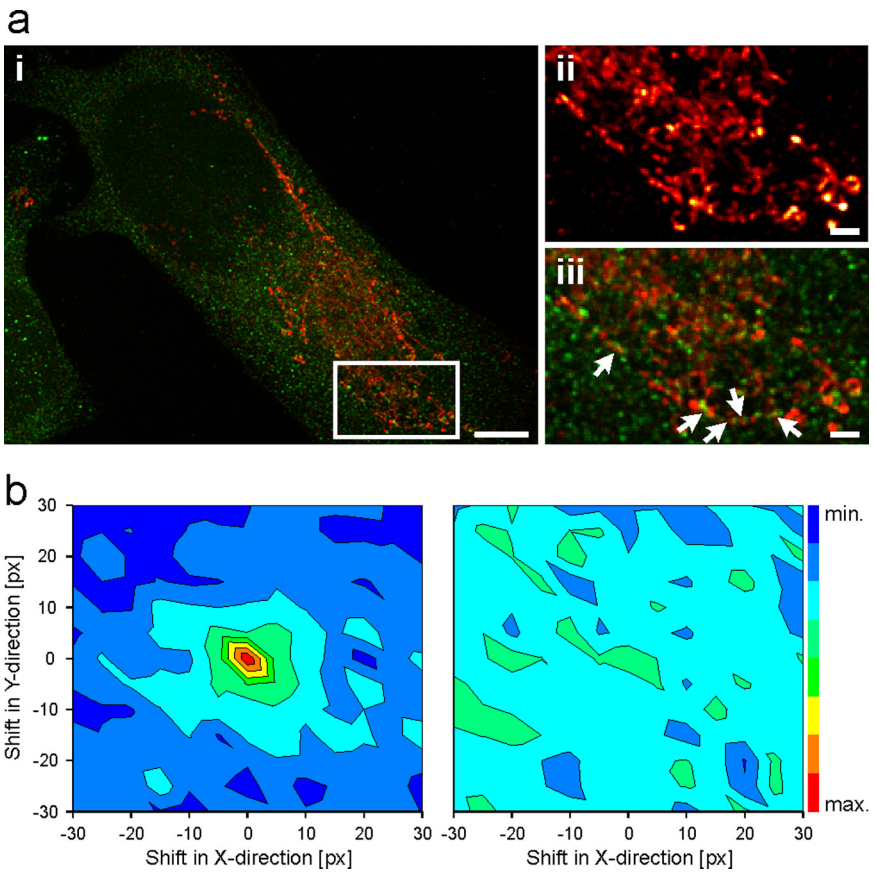

FIG 5 Kinesin-1 colocalizes with SseJ clusters in PFA-fixed cells. (a) (i) Dual-color spinning-disk SIM image of an infected HeLa cell, 12 h after invasion, fixed in PFA and stained for SseJ-HA (red) and kinesin (green). (ii and iii) Magnified view of SseJ-HA structures and kinesin of the boxed region in panel i (arrows [iii] indicate colocalization). Bars, 5 μm (i) and 1 μm (ii and iii). (b) Colocalization analysis was performed by calculating the Manders M1 coefficient (kinesin colocalizing with SseJ) for the original dual-color image ($x = y = 0$) and for control images generated by translating the spectral channels with respect to each other in x and y directions (see Materials and Methods). This analysis generates a colocalization map, with a peak intensity at $x = y = 0$ indicating true colocalization (left diagram, $n = 5$ cells). Colocalization analysis of mock-infected cells (right diagram, $n = 5$ cells) stained for kinesin and SseJ-HA showed no peak intensity at $x = y = 0$, indicating that there was no colocalization of nonspecifically bound anti-HA antibodies and kinesin. The same color map scaling was used for comparison. px, pixels.

In summary, the pearling transition or instability, which is a sequential beading of tubular vesicles, can be exploited for understanding the mechanism of how *Salmonella*-induced filaments form. In the present work, we demonstrate that SseJ is subject to the pearling instability; at high osmolality, it appears as periodic clusters of uniform size (Fig. 1 and 2). During fixation at low osmolality, in which microtubule structures are preserved, pearls of SseJ are no longer evident; instead, SseJ is visible as a continuous filament (Fig. 4). The pearling transition reveals a force-dependent process that drives endosomal tubulation, and here we identify kinesin as the motor that supplies this force.

MATERIALS AND METHODS

Bacterial strains and culture conditions. *Salmonella enterica* serovar Typhimurium strain NCTC12023 was the wild-type strain, and various isogenic mutants are described in the text. Bacteria were grown overnight in LB broth at 37°C with shaking.

Mammalian cell culture and host cell infection. The nonpolarized human epithelial cell line HeLa (American Type Culture Collection; ATCC CCL-2) was used for *Salmonella* infections. HeLa cells were maintained in high-glucose (4.5-g/liter) Dulbecco's modified Eagle's medium (DMEM) containing glutamine and pyruvate (Thermo Fisher) and supplemented with 10% inactivated fetal bovine serum (FBS; Thermo Fisher) at 37°C and antibiotics (antibiotic-antimycotic final 5× stock; Thermo Fisher) in a humidified 5% CO_2 incubator. The cells were gently trypsinized with Accutase (StemPro Accutase; Thermo

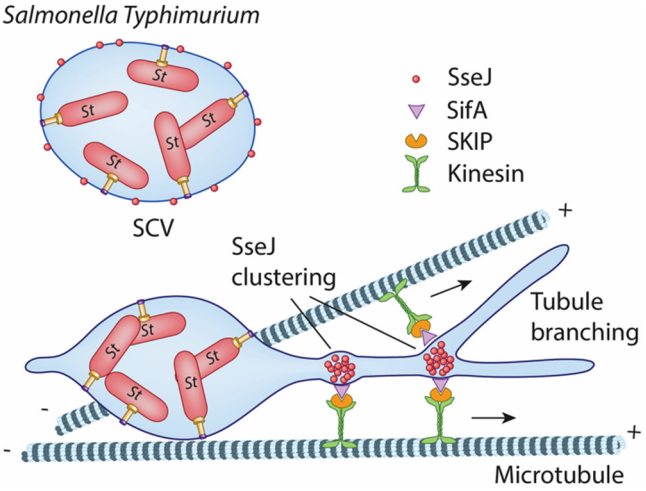

FIG 6 Summary of SPI-2 secretion and endosomal tubule (SIF) formation. (Top) *Salmonella* is shown in an acidic vacuole. EnvZ sensing and upregulation of the SsrA/B system occur upon acidification of the *Salmonella* cytoplasm (2, 25). (Bottom) Secretion of effectors SifA and SseJ leads to SseJ clustering (in the case of PFA fixation) on the outside of SIFs and colocalization with tubulin. Clustering is driven by the motor protein kinesin, which is colocalized with SseJ. In the absence of SifA, SseJ surrounds the vacuole and destabilizes it (top panel).

Fisher), and ~2 × 10^4 cells were seeded in an 8-chambered slide with a glass bottom from Sarstedt (Germany) and allowed to grow 24 h before infection.

Infections. *S.* Typhimurium was cultured overnight in standard LB broth. Overnight cultures were subcultured in 3 ml LB for 3.5 to 4 h (optical density at 600 nm [OD_{600}], ~2-3). The cultures were then diluted to an OD_{600} of 0.2. HeLa cells were infected with a multiplicity of infection (MOI) of 100:1 (bacteria/HeLa cell) and bacteria were internalized for 30 min. Subsequently, the remaining extracellular bacteria were removed by washing the cells three times in Dulbecco's phosphate-buffered saline (DPBS), followed by incubation with 100 μg/ml of gentamicin for 1 h in DMEM with 10% FBS. The cells were again washed three times with DPBS and further incubated in DMEM with 10% FBS and gentamicin (10 μg/ml) for the rest of the infection. Cells were fixed for imaging at different time points postinfection as described below.

Cell fixation. Cells were fixed using 200 μl of methanol-free 4% PFA (electron microscopy [EM] grade; TaKaRa) in PBS. Cells were fixed for 10 min, washed twice with PBS, and resuspended in 300 μl PBS. For tubulin-conserving fixation, cells were extracted for 1 min using a microtubule-stabilizing buffer (MTSB) containing 80 mM PIPES [piperazine-*N*,*N*′-bis(2-ethanesulfonic acid)], pH 6.8, 1 mM $MgCl_2$, 5 mM EGTA, and 0.5% Triton X-100. The buffer was exchanged with MTSB containing 0.2% GA, and cells were fixed for 10 min at room temperature (RT). Excess GA was quenched for 6 min using 0.2% sodium borohydrate in PBS, which was freshly prepared directly before use. After several washes with PBS, cells were processed for immunostaining.

Immunostaining. Primary antibody solution (200 μl) was added to each chamber, followed by a 1-h incubation at RT. The antibody solution is a PBS-based buffer containing 5% bovine serum albumin (BSA) and 0.1% saponin. For the staining of secreted SseJ, the rabbit/mouse anti-HA primary antibody (Sigma; H6908 and H9658) was used (rabbit, 1:500 dilution, and mouse, 1:300 dilution). Rabbit monoclonal anti-KIF5B (Abcam catalog no. ab167429) was used for kinesin, and a monoclonal mouse anti-LAMP-1 primary antibody (Santa Cruz Biotechnology; clone H4A3, 0.4 μg/ml) was used for LAMP-1. The antibody solution was removed, and cells were gently washed three times with PBS containing 0.1% Tween 20. Secondary antibody (donkey anti-rabbit 647 [Thermo Fisher catalog no. A-31573], goat anti-rabbit 488 [catalog no. A-11034], goat anti-mouse 568 [catalog no. A11004], and goat anti-mouse AF532 [catalog no. A-11002], 2 μg/ml) diluted at 1:500 in PBS-BSA-saponin buffer (see above) was subsequently added for 1 h at room temperature in the dark. After three washing steps (see above), 4′,6-diamidino-2-phenylindole (DAPI; 600 nM in PBS) solutions were applied for 10 min to stain HeLa cell and *Salmonella* DNA. After completed staining, Tetraspeck FluoSpheres (Thermo Fisher; 1:500 in PBS) or gold nanorods (Nanopartz; 25 by 65 nm; catalog no. C12-25-650-TNHS; 1:500 in PBS) were added to the sample for 10 min. Nonadhered beads were washed off gently using PBS. The cells were stored in PBS in the dark at 4°C.

Confocal laser scanning microscopy. Confocal imaging was performed on a commercial microscope (LSM 710; Zeiss, Germany) equipped with a Plan-Apo 63× oil objective (1.4 numerical aperture [NA]; Zeiss). Alexa Fluor 647 was imaged using 633-nm excitation. Alexa Fluor 532 was imaged using a 532-nm laser line of an external argon-ion laser (LGN3001; Lasos Lasertechnik GmbH, Germany). DAPI was imaged with 405-nm UV-light excitation (Coherent Cube 405-100C; Coherent, USA), coupled into the microscope via an optical fiber. Filter sets were selected to match the excitation and emission properties of the fluorophores. Images were recorded in sequential mode using a pixel size of 100 nm and 2× line averaging.

SMLM imaging. *d*STORM measurements were carried out on a home-built microscope as described previously (26), using dichroic mirrors (HC Quad 410/504/582/669 or HC Dualband 560/659, both from Semrock) and emission filters (700/75 ET band-pass or 570/60 ET band-pass, both from Chroma) adapted for single-molecule imaging of Alexa Fluor 647 and Alexa Fluor 532. Images were recorded with an electron-multiplying–charge-coupled device (EMCCD) camera (iXon Ultra, DU-897U-CS0-#BV; Andor Technology), using the following settings: 10-MHz readout frequency, a preamplifier gain of 3, an electron-multiplying gain of 200, and a frame rate of 33 Hz. An imaging buffer (100 mM Tris, pH 8.5, 100 mM 2-mercaptoethylamine hydrochloride [MEA; Sigma-Aldrich], and 10 mM NaCl) was prepared freshly prior to SMLM imaging. At first, the DAPI signal was recorded using 405-nm laser excitation (50 camera frames). *d*STORM imaging of Alexa Fluor 647 was subsequently performed using the 647-nm laser line of a Coherent Innova 70C Spectrum multiline Ar/Kr mixed-gas laser (2.5 W; Coherent) at 3 kW/cm^2 and low UV excitation densities (up to 10 W/cm^2) for fluorophore reactivation and minimal photobleaching of Alexa Fluor 532 molecules. Alexa Fluor 532 was photoswitched using 532-nm laser excitation at ~2.2 kW/cm^2. Typically, 15,000 images were recorded for each spectral channel.

Data analysis. SMLM data were analyzed with rapidSTORM v. 3.31 (27). Single-molecule signals were fitted using the Levenberg-Marquardt fitting routine based on a global threshold, keeping the full width at half maximum (FWHM) of the point spread function as a free-fitting parameter. Localizations were subsequently filtered according to their FWHM in *x* and *y* directions, and signals with widths between 220 nm and 540 nm and an FWHM ratio between 0.7 and 1.3 (symmetry filter) were maintained. A photon threshold of 150 photons (Alexa Fluor 532) or 200 photons (Alexa Fluor 647) was applied. Molecules that emitted over multiple frames were grouped into a single localization. Reconstructed images were processed in Fiji (28): a Gaussian filter with a sigma of 10 nm was applied, and brightness and contrast were adjusted for each channel for optimal visualization. Fiducial markers were used to correct for drift. Linear drift was quantified using fast-Fourier transformation (FFT) and subsequent correction in rapidSTORM. Nonlinear drift was corrected using custom-written software (29). The displacement between SseJ-HA and LAMP-1 channels was determined using the ImageJ plugin "2D Stitching" (100 peaks windowing) (30) and corrected in Fiji (28).

Determination of SseJ cluster spacings and SIF diameters. For the analysis of SseJ cluster spacing in PFA-fixed samples, "pearls-on-a-string" structures were manually selected using the segmented line tool in Fiji (spline interpolation). Intensity profiles were generated using the plugin "Plot Profile" tool with a line width of 500 nm. For visualization, selections were linearized using the plugin "Straighten." Intensity profiles were fitted with a multicomponent Gaussian function using OriginPro 9.1 G (OriginLab). The spacing between two neighboring SseJ clusters was determined as the centroid distance of the Gaussian fits. SIF diameters were determined similarly, using intensity profiles of SIF cross sections with 0.4- to 1-μm width. A two-component Gaussian fit function was applied, yielding the SIF diameter as the Gaussian interpeak distance.

Structured-illumination microscopy. SIM imaging was performed on a W1 spinning-disk microscope (CSU-W1; Nikon, Japan) combined with the Live-SR system (Roper Scientific) and equipped with a Plan-Apo λ 100$\times$ oil objective (1.45 NA; Nikon, Japan). Excitation and band-pass filters were as follows: DAPI was imaged with a 405-nm laser and emission of 445/45 nm, Alexa Fluor 488 was imaged using 488-nm excitation and emission of 525/30 nm, and Alexa Fluor 568 was imaged using 561-nm excitation and emission of 617/73 nm. Three-dimensional (3D) image stacks of whole cells were acquired with a scalable complementary metal-oxide semiconductor (sCMOS) camera (Prime 95B; Photometrics, USA), using an image pixel size of 78.96 nm by 78.96 nm (1,200 by 1,200 pixels) and an 0.2-μm z-stack step size. The raw images were processed to superresolution images by using the Live-SR algorithm reported by York et al. (21).

Colocalization analysis. Colocalization between SseJ-HA and kinesin was determined from dual-color SIM images using a variation of Manders' colocalization analysis (22) and Fiji (28). The maximum-intensity projections of both spectral channels were first converted into a binary image using Otsu's algorithm. Colocalizing pixels were identified by multiplying the binary images. In order to discriminate random overlap and true colocalization, one image channel (kinesin) was translated in *x*, *y* using a custom-written macro in Fiji. For each translation step, the M1 (kinesin colocalizing with SseJ) and M2 (SseJ colocalizing with kinesin) values of the two images were calculated. Colocalization maps were created using OriginPro 9.1G. One to 3 regions of interest (ROIs) per cell ($n = 5$ cells) were analyzed. The M1 value for each ROI was normalized (division by maximum value), followed by averaging of all M1 values. The heterogeneity of both *Salmonella* infection and SseJ secretion strongly influences the absolute values of the Manders coefficients. Normalization of colocalization maps was hence required prior to averaging to prevent masking of existing colocalization.

SUPPLEMENTAL MATERIAL

Supplemental material for this article may be found at https://doi.org/10.1128/mBio.01083-18.

FIG S1, PDF file, 1.1 MB.

FIG S2, PDF file, 2.1 MB.

FIG S3, PDF file, 0.5 MB.

ACKNOWLEDGMENTS

We acknowledge the technical expertise of Roopa Rajashekar with infections and M. P. Sheetz and Jacques Prost for helpful discussions regarding the pearling transition.

We are extremely grateful to Felix Margadant for extraordinary assistance with data recovery; we also acknowledge the superb expertise of the Mechanobiology Microscopy Core Facility.

This work was supported by a Research Center of Excellence in Mechanobiology from the Ministry of Education, Singapore, VA1IOBX-000372, and NIH AI-123640 to L.J.K. M.H. and C.S. were supported by the German Science Foundation (EXC 115 and SFB902) and Goethe-University Frankfurt.

REFERENCES

1. Drecktrah D, Knodler LA, Howe D, Steele-Mortimer O. 2007. Salmonella trafficking is defined by continuous dynamic interactions with the endolysosomal system. Traffic 8:212–225. https://doi.org/10.1111/j.1600-0854.2006.00529.x.
2. Chakraborty S, Mizusaki H, Kenney LJ. 2015. A FRET-based DNA biosensor tracks OmpR-dependent acidification of Salmonella during macrophage infection. PLoS Biol 13:e1002116. https://doi.org/10.1371/journal.pbio.1002116.
3. Stein MA, Leung KY, Zwick M, Garcia-del Portillo F, Finlay BB. 1996. Identification of a Salmonella virulence gene required for formation of filamentous structures containing lysosomal membrane glycoproteins within epithelial cells. Mol Microbiol 20:151–164. https://doi.org/10.1111/j.1365-2958.1996.tb02497.x.
4. Ohlson MB, Fluhr K, Birmingham CL, Brumell JH, Miller SI. 2005. SseJ deacylase activity by Salmonella enterica serovar Typhimurium promotes virulence in mice. Infect Immun 73:6249–6259. https://doi.org/10.1128/IAI.73.10.6249-6259.2005.
5. Ohlson MB, Huang Z, Alto NM, Blanc MP, Dixon JE, Chai J, Miller SI. 2008. Structure and function of Salmonella SifA indicate that its interactions with SKIP, SseJ, and RhoA family GTPases induce endosomal tubulation. Cell Host Microbe 4:434–446. https://doi.org/10.1016/j.chom.2008.08.012.
6. Heilemann M. 2010. Fluorescence microscopy beyond the diffraction limit. J Biotechnol 149:243–251. https://doi.org/10.1016/j.jbiotec.2010.03.012.
7. Spahn C, Glaesmann M, Gao Y, Foo YH, Lampe M, Kenney LJ, Heilemann M. 2017. Sequential super-resolution imaging of bacterial regulatory proteins, the nucleoid and the cell membrane in single, fixed E. coli cells. Methods Mol Biol 1624:269–289. https://doi.org/10.1007/978-1-4939-7098-8_20.
8. Boucrot E, Beuzón CR, Holden DW, Gorvel JP, Meresse S. 2003. *Salmonella typhimurium* SifA effector protein requires its membrane-anchoring C-terminal hexapeptide for its biological function. J Biol Chem 278:14196–14202. https://doi.org/10.1074/jbc.M207901200.
9. McGourty K, Thurston TL, Matthews SA, Pinaud L, Mota LJ, Holden DW. 2012. Salmonella inhibits retrograde trafficking of mannose-6-phosphate receptors and lysosome function. Science 338:963–967. https://doi.org/10.1126/science.1227037.
10. Ruiz-Albert J, Yu XJ, BeuzÓn CR, Blakey AN, Galyov EE, Holden DW. 2002. Complementary activities of SseJ and SifA regulate dynamics of the Salmonella typhimurium vacuolar membrane. Mol Microbiol 44:645–661. https://doi.org/10.1046/j.1365-2958.2002.02912.x.
11. Dabora SL, Sheetz MP. 1988. The microtubule-dependent formation of a tubulovesicular network with characteristics of the ER from cultured cell extracts. Cell 54:27–35. https://doi.org/10.1016/0092-8674(88)90176-6.
12. Ho JC, Rangamani P, Liedberg B, Parikh AN. 2016. Mixing water, transducing energy, and shaping membranes: autonomously self-regulating giant vesicles. Langmuir 32:2151–2163. https://doi.org/10.1021/acs.langmuir.5b04470.
13. Yanagisawa M, Imai M, Taniguchi T. 2008. Shape deformation of ternary vesicles coupled with phase separation. Phys Rev Lett 100:148102. https://doi.org/10.1103/PhysRevLett.100.148102.
14. Pullarkat PA, Dommersnes P, FernÁndez P, Joanny JF, Ott A. 2006. Osmotically driven shape transformations in axons. Phys Rev Lett 96:048104. https://doi.org/10.1103/PhysRevLett.96.048104.
15. DerÉnyi I, Jülicher F, Prost J. 2002. Formation and interaction of membrane tubes. Phys Rev Lett 88:238101. https://doi.org/10.1103/PhysRevLett.88.238101.
16. Rajashekar R, Liebl D, Chikkaballi D, Liss V, Hensel M. 2014. Live cell imaging reveals novel functions of Salmonella enterica SPI2-T3SS effector proteins in remodeling of the host cell endosomal system. PLoS One 9:e115423. https://doi.org/10.1371/journal.pone.0115423.
17. Boucrot E, Henry T, Borg JP, Gorvel JP, MÉresse S. 2005. The intracellular fate of Salmonella depends on the recruitment of kinesin. Science 308:1174–1178. https://doi.org/10.1126/science.1110225.
18. Whelan DR, Bell TD. 2015. Super-resolution single-molecule localization microscopy: tricks of the trade. J Phys Chem Lett 6:374–382. https://doi.org/10.1021/jz5019702.
19. Krieger V, Liebl D, Zhang Y, Rajashekar R, Chlanda P, Giesker K, Chikkaballi D, Hensel M. 2014. Reorganization of the endosomal system in Salmonella-infected cells: the ultrastructure of Salmonella-induced tubular compartments. PLoS Pathog 10:e1004374. https://doi.org/10.1371/journal.ppat.1004374.
20. Sanborn J, Oglecka K, Kraut RS, Parikh AN. 2013. Transient pearling and vesiculation of membrane tubes under osmotic gradients. Faraday Discuss 161:167–176, 273–303. https://doi.org/10.1039/C2FD20116J.
21. York AG, Chandris P, Nogare DD, Head J, Wawrzusin P, Fischer RS, Chitnis A, Shroff H. 2013. Instant super-resolution imaging in live cells and embryos via analog image processing. Nat Methods 10:1122–1126. https://doi.org/10.1038/nmeth.2687.
22. Manders EMM, Verbeek FJ, Aten JA. 1993. Measurement of co-localization of objects in dual-colour confocal images. J Microscopy 169:375–382. https://doi.org/10.1111/j.1365-2818.1993.tb03313.x.
23. Bar-Ziv R, Tlusty T, Moses E. 1997. Critical dynamics in the pearling instability of membranes. Phys Rev Lett 79:1158–1161. https://doi.org/10.1103/PhysRevLett.79.1158.
24. Raines SA, Hodgkinson MR, Dowle AA, Pryor PR. 2017. The Salmonella effector SseJ disrupts microtubule dynamics when ectopically expressed in normal rat kidney cells. PLoS One 12:e0172588. https://doi.org/10.1371/journal.pone.0172588.
25. Chakraborty S, Winardhi RS, Morgan LK, Yan J, Kenney LJ. 2017. Non-canonical activation of OmpR drives acid and osmotic stress responses in single bacterial cells. Nat Commun 8:1587. https://doi.org/10.1038/s41467-017-02030-0.
26. Spahn C, Cella-Zannacchi F, Endesfelder U, Heilemann M. 2015. Correlative super-resolution imaging of RNA polymerase distribution and dynamics, bacterial membrane and chromosomal structure in Escherichia coli. Methods Appl Fluoresc 3:014005. https://doi.org/10.1088/2050-6120/3/1/014005.
27. Wolter S, Schüttpelz M, Tscherepanow M, van de Linde S, Heilemann M, Sauer M. 2010. Real-time computation of subdiffraction-resolution fluorescence images. J Microsc 237:12–22. https://doi.org/10.1111/j.1365-2818.2009.03287.x.
28. Schindelin J, Arganda-Carreras I, Frise E, Kaynig V, Longair M, Pietzsch T, Preibisch S, Rueden C, Saalfeld S, Schmid B, Tinevez JY, White DJ, Hartenstein V, Eliceiri K, Tomancak P, Cardona A. 2012. Fiji: an open-source platform for biological-image analysis. Nat Methods 9:676–682. https://doi.org/10.1038/nmeth.2019.
29. Malkusch S, Heilemann M. 2016. Extracting quantitative information from single-molecule super-resolution imaging data with LAMA-LocAlization Microscopy Analyzer. Sci Rep 6:34486. https://doi.org/10.1038/srep34486.
30. Preibisch S, Saalfeld S, Tomancak P. 2009. Globally optimal stitching of tiled 3D microscopic image acquisitions. Bioinformatics 25:1463–1465. https://doi.org/10.1093/bioinformatics/btp184.